# ELECTROSPUN/ELECTROSPRAYED ALIGNED FUEL CELL ELECTRODES

A Thesis

by

ARTHUR CONRAD KLEIDERER IV

Submitted to the Office of Graduate and Professional Studies of
Texas A&M University
in partial fulfillment of the requirements for the degree of

MASTER OF SCIENCE

Chair of Committee, Yossef A. Elabd
Committee Members, Jodie L. Lutkenhaus
Partha Mukherjee

Head of Department, M. Nazmul Karim

August 2017

Major Subject: Chemical Engineering

Copyright 2016 Arthur Conrad Kleiderer IV

## ABSTRACT

Proton exchange membrane fuel cells (PEMFCs) are a promising technology in energy conversion. However, the high cost of the platinum catalyst limits the use of fuel cells. To address this problem, many improvements and optimizations have been proposed for the PEMFC catalyst layer. In this study, an apparatus to produce aligned Nafion fiber catalyst layers is designed, the alignment capabilities of the apparatus are explored, and the performance of the aligned catalyst layer is evaluated.

A horizontal accelerated drum is able to produce aligned Nafion fibers up to 80% alignment. This alignment is present at drum speeds over 3000 rpm over a wide range of electrospinning solution flow rates. A catalyst layer fabricated *via* simultaneous electrospinning and electrospraying (E/E) has a peak power density of 535 mW $cm^{-2}$ and an electrochemical surface area of 42 $m^2$ $g_{Pt}^{-1}$. This performance is comparable to the performance of a randomly aligned catalyst layer fabricated with E/E.

## CONTRIBUTORS AND FUNDING SOURCES

### Contributors

This work was supervised by a thesis committee consisting of Professor Yossef Elabd, advisor, and Professor Jodie Lutkenhaus of the Department of Chemical Engineering and Professor Partha Mukherjee of the Department of Mechanical Engineering.

All work for the thesis was completed independently by the student.

### Funding Sources

There are no outside funding contributions to acknowledge related to the research and compilation of this document.

## TABLE OF CONTENTS

Page

## LIST OF FIGURES

Page

# 1. INTRODUCTION AND LITERATURE REVIEW

## 1.1. Proton Exchange Membrane Fuel Cells

Proton exchange membrane fuel cells (PEMFCs) are a promising technology for energy conversion due to their high energy density, zero-emissions, and fast refuel. Proposed applications include small portable electronics and large moving vehicles. PEMFCs offer advantages over an energy storage device, such as a lithium-ion battery, by providing a higher overall energy density and fast refueling. The invention of fuel cells is attributed to Sir William Grove in 1839.[1] The first notable use of a PEMFC is by NASA in the Gemini space shuttle.[2] Since this time, many companies, specifically car manufacturers, have invested into fuel cell research.[3] The largest drawback of a PEMFC is the need for significant amounts of expensive platinum catalyst to facilitate the oxygen reduction reaction at low operating temperatures.[4] This inhibits the economic viability of PEMFCs as a competitor to current energy storage and conversion technologies. Current research is aimed at reducing or eliminating the required platinum in the fuel cell.

Figure 1.1 shows a basic schematic of a PEMFC. The catalyst layer is provided the reactions *via* gas channels in the current collector. The anode is fed hydrogen and the cathode is fed oxygen in the form of either pure oxygen or air. The gas then diffuses through the gas diffusion layer (GDL), which serves to distribute the reactant evenly across the catalyst layer. In the anode, protons and electrons are generated. The protons pass through the proton exchange membrane (PEM), which is most commonly made of a DuPont product called Nafion. These protons then react with the oxygen and electrons in

the cathode catalyst layer to form water. The electrons from the anode cannot pass through the insulating membrane and are forced through an external circuit before arriving at the cathode current collector.

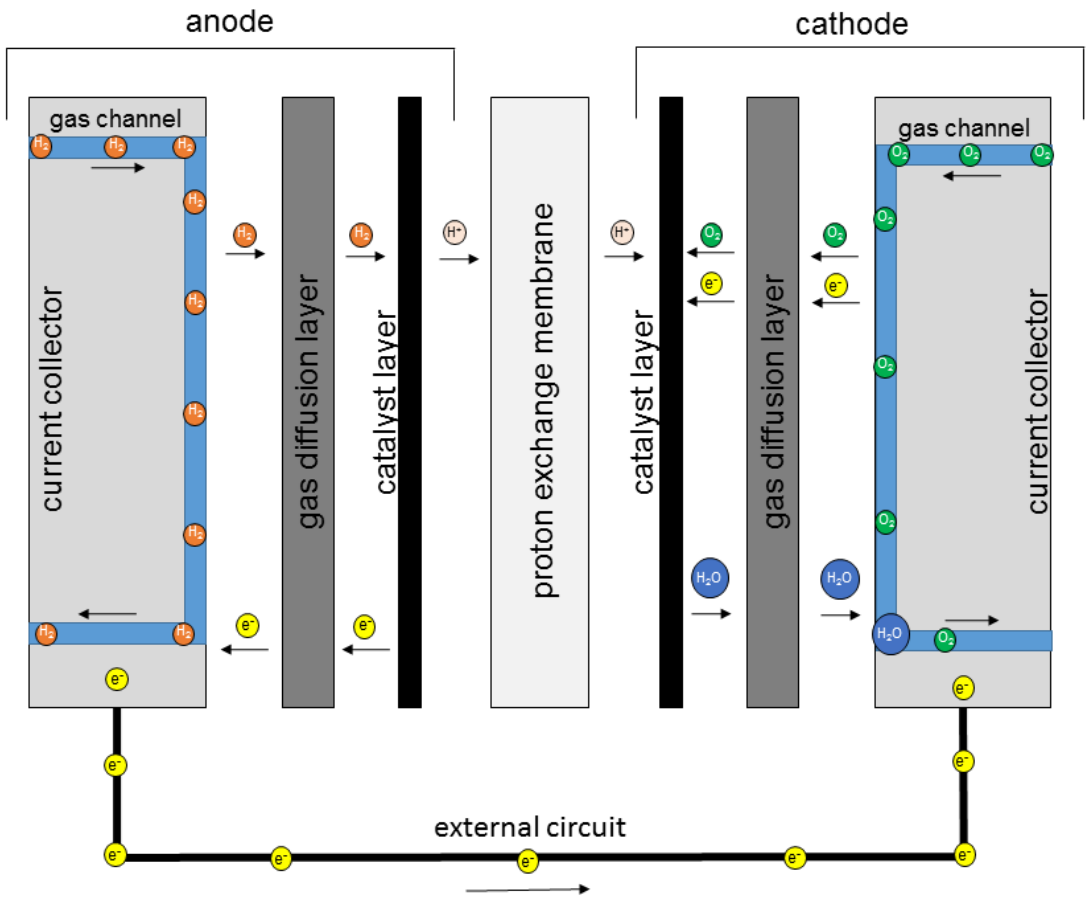


**Figure 1.1** Schematic of proton exchange membrane fuel cell.

The catalyst layer contains the catalyst, electron conductors, and proton conductors. Typically, the catalyst is platinum on a carbon support. The carbon support also functions as the electron conductor. The proton conductor is most commonly Nafion. The morphology of these components must facilitate the transport of the reactant gas, protons, and electrons to available catalyst sites and water out of the cell. Points in the structure which allow for all of three reactants to meet are referred to as a triple phase boundary (TPB). An ideal catalyst layer has a large number of TPBs and low tortuosity for each of the transported components. Optimization of the catalyst layer focuses on finding optimal morphologies which meet the above requirements.

## 1.2. Nanoscale Electrode Fabrication

In 2002, Middelman [5] observed the formation of nanofiber structures formed in the catalyst layer and proposed an ideal membrane consisting of perpendicular nanofibers constructed of a catalyst core and proton conductor shell with channels for gas and water transport in between. He was able to produce such structures in electrodes by using a strong electric field as a driving force.[5] Our laboratory later showed that nanofibers form under normal operating conditions in the fuel cell.[6] Further investigation showed that these fibers form at temperatures above 60 °C and result in increased performance of the cell regardless of operating temperature.[6] This work demonstrates the improvements possible by exploring nanoscale morphologies.

First efforts to produce nanoscale electrode structures used the electrospraying technique.[7-9] Baturina and Wnek electrosprayed the electrode material directly on to the

Nafion membrane and reported good initial results, but the MEA exhibited high transport resistance in the gas phase, resulting in decreased performance at high current densities.[7] Improvements in the electrospraying method have focused on improving the composition of ionomer and catalyst in the spray solution,[10-11] solvent properties,[12] and deposition of the particles.[13]

Chaparro *et al.*[10] explored the optimal composition of the spray solution. They concluded that a Nafion concentration of 15% was optimal based on a minimum in observed internal resistance in the cell. This ionomer concentration was also close to the maximum in Pt utilization. Similarly, for Pt loadings, an optimum of 0.17 mg $cm^{-2}$ was reported.

Martin *et al.* [11] pursued similar work, but explored lower loadings of Pt from 0.1 to 0.0125 mg $cm^{-2}$. They observed that the optimal Nafion concentrations for electrospraying increased as they lowered the Pt loading. Based on performance, they reported an optimal Nafion concentration of 30% at 0.1 mg $cm^{-2}$, 40% at 0.05 mg $cm^{-2}$, and 50% at 0.025 mg $cm^{-2}$.

Martin *et al.*[13-14] also demonstrated the effects of the Pt weight percent of the catalyst particle. In two separate papers, they report the Pt utilization at 0.01 mg $cm^{-2}$. In the first they used a 20% Pt/C catalyst and observed 20 kW $g_{Pt}^{-1}$. The second paper used a 10% Pt/C catalyst and observed 30 kW $g_{Pt}^{-1}$.

Electrospinning has also been explored as a method for fabricating electrodes. Chen *et al.*[15] studied Nafion in solution and demonstrated a method to electrospin the Nafion to produce nanofibers. This work studied the aggregate sizes of Nafion in solution in a range

of solvents and showed that Nafion polymer chains do not entangle sufficiently to electrospin by itself. To solve this, Chen demonstrated that the addition of poly(acrylic) acid (PAA) decreased the hydrodynamic radius of the aggregates in solution allowing the solution to electrospin.[15]

The Pintauro group used this method combined with a Pt/C catalyst to form electrospun electrodes.[16-17] In their first work, a Nafion/PAA/Pt/C nanofiber electrode was reported and compared to a control MEA. They showed an increase in ECSA from 60 $m^2\ g_{Pt}^{-1}$ in the control MEA to 114 $m^2\ g_{Pt}^{-1}$ in the electrospun MEA. They also showed improved durability of the MEA in cyclic stability testing.[17] Following up their first work, the Pintauro group reported the performance over a wider variety of operating conditions, including a peak power of 906 mW $cm^{-2}$ at 80 °C, 3 atm back pressure, and fully humidified gas flow rates of 500 and 2000 sccm of $H_2$ and air, respectively.[16]

In our group, Wang *et al*. used simultaneous electrospinning and electrospraying (E/E) to fabricate a fuel cell catalyst layer.[18] This method allows for the advantages of electrosprayed catalyst, while also maintaining porosity. Wang reported high performance, at platinum loadings as low as 0.022 $mg_{Pt,cath}\ cm^{-2}$ with a Pt utilization of over 40 kW $g_{Pt}^{-1}$.[18] Improving on this work, Wang also showed that a small amount of polytetrafluoroethylene (PTFE) added to the catalyst layer was sufficient to improve the performance of the MEA significantly, resulting in over 30% improvement in the platinum utilization.[19] Wang's work demonstrates the viability of E/E as a method for producing catalyst layers with highly tunable properties. Because of the flexibility this method provides, there exists many opportunities to further optimize the catalyst layer

morphology. One of these methods would be to use the spun fibers as a template to create patterns in the layer. This could then allow for optimization of channels for gas and liquid water transport, while maintaining high electron and ionic conductivity.

### 1.3. Controlled Electrospinning Fabrication

There have been many methods reported in the literature that exercise some degree of control over the deposition pattern of electrospun nanofibers. By far, the most common is fiber alignment and has been achieved by several means including rotating drum [20-22], parallel plates [23-24], and magnetic fields [25].

All of these options have their own strengths and weaknesses. Li *et al.* [23] successfully demonstrated that parallel plates are effective in the production of aligned fibers and that multiple electrode pairs can be used in series to fabricate more complex structures. However, the alignment is dependent on the distance of the gap and the requirement of an insulating medium between the electrodes.[23]

Liu *et al.* [25] used a magnetic field to fabricate aligned straight and wavy fibers without any addition of magnetic particles. They spun poly(D,L-lactic-co-glycolic acid) (PLGA) for collection times up to 2 hours and demonstrated that thick mats are possible without losing the alignment. This technique is dependent on the presence of a gap between the magnets and the size of that gap.[25]

Matthews *et al.* [20] demonstrated the use of a rotating drum assembly to align collagen fibers. They showed that at a surface velocity of 1.4 m $s^{-1}$, the collagen fibers were highly

aligned in the direction of rotation.[20] The rotating drum has the advantage of high collection area, which can be further enhanced by moving the spinning needle.

There have been methods reported, which can control the fiber deposition beyond simple alignment. These methods include dynamic electrical fields[26] and near-field electrospinning.[27-29] These techniques demonstrate that the creation of more complex fiber structures is possible.

In this work, several apparatus were designed and utilized to explore the viability of each for fabricating aligned Nafion fibers in an E/E catalyst layer. The parameters of the apparatus are then explored to find the ideal process parameters for alignment. Finally, the fuel cell performance of an aligned fiber E/E catalyst layer is compared with a randomly orientated catalyst layer.

# 2. DESIGN OF EXPERIMENTAL APPARATUS

## 2.1. Introduction

In this work, both magnetic field assisted-electrospinning and accelerated rotating drum speeds were explored to determine the suitability for fabrication of a PEMFC catalyst layer. Priority is placed on both achieving high alignment in fiber mats and creating large area uniform catalyst layers.

## 2.2. Experimental Methods

### 2.2.1. Materials

Isopropanol (99.5%, Sigma Aldrich), Nafion solution (1100 EW, 5 wt% in a 3:1 v:v of isopropanol/water, Ion Power), poly(acrylic acid) (PAA; $M_V$ = 450,000 g $mol^{-1}$, Sigma Aldrich), 20 wt% platinum on carbon catalyst (Pt/C; Vulcan XC-72, Premetek Co.), 60 wt% platinum on carbon catalyst (60% Pt/C; Vulcan XC-72, Premetek Co.), were used as received. Ultrapure deionized (DI) with resistivity greater than 16 MΩ·cm (25 °C) was used as appropriate.

### 2.2.2. Fiber Characterization

Scanning electron microscopy (SEM; FEI Quanta 600 FE-SEM; 5 kV; working distance = 10 cm) was used to investigate the morphology of the fibers. The samples were removed from the collector after spinning. Samples were sputter coated (Cressington 208 HR) with platinum/palladium (thickness = 10 nm).

Image analysis was performed using ImageJ software to characterize the fiber diameter and orientation. DiameterJ was used to segment the image and calculate the diameter of the fibers. OrientationJ was utilized to obtain the orientation distribution of the fibers. This distribution was converted to an overall percentage *via* the method reported by Rahmani *et al.*[30] This method uses the relative frequencies in the histogram and weighs them based on the distance from the target orientation. This method will assign a value of 100% aligned to a sample completely aligned in the target direction, 0% aligned to a sample completely aligned perpendicular to the target direction, and 33% aligned to a sample with completely random alignment. In this work, the target direction was always chosen as the orientation, which provided the best fit of the histogram to a normal curve.

### 2.2.3. Preparation of Solutions

The electrospinning solution used for the creation of fiber mats was fabricated with the following specifications. 18.75 mg of PAA, 1500 mg of Nafion solution, and 375 mg of isopropanol/water (3/1 v/v) were added to obtain a 5% by weight in the polymer solution. The resulting solution contained a 4/1 w/w Nafion/PAA ratio. The solution was allowed to stir for several hours until PAA was completely dissolved.

The electrospraying solution was fabricated by adding 40 mg of 20% Pt/C, 32 mg of Nafion at 5% of the carbon weight, and 3.9 g isopropanol/water (3/1 v/v ) to reach 1% solids in the solution. The solution was then sonicated (duration = 5 min, amplitude = 35%; Model CL-18, Qsonica Sonicator) to disperse the Pt/C.

The Pt/C electrospinning solution was produced similar to previous work by the Pintauro group.[17] This solution eliminates the need for electrospraying adding the catalyst to the electrospinning solution. The Pt/C solution was created by adding 40 mg of 60% Pt/C, 425.5 mg of Nafion solution, and 6.8 mg of PAA, resulting in a final ratio of 47:500:8 w/w/w 60% Pt/C/Nafion solution/PAA. The solution was stirred to dissolve the PAA and then sonicated (duration = 15 min, amplitude = 35%) prior to disperse the Pt/C.

### 2.2.4. Magnetic Field Apparatus

Figure 2.1 shows a schematic of the magnetic field apparatus developed. Neodymium ring magnets (o.d. = 4 in., i.d. = 2 in, thickness = 1 in.; Apex Magnets) were placed on a poly(vinyl chloride) (PVC) tube (i.d. = 1.61 in, o.d. = 1.9). The magnet was held in place by steel clamps (i.d. = 1.94 in.; McMaster-Carr). Acetyl resin rings were used as spacers to ensure accurate distance between magnets (i.d. = 2, o.d. = 3 in., thickness = 0.5 – 3 cm; custom). The assembly was driven by a motor (Model 4IK25GN-SW2, Oriental Motor). On either side of the assembly, two high-voltage power supplies (Model PS/EL50R00.8, Glassman High Voltage, Inc. and Model ES40P-10W/DAM, Gama High Voltage Research) supplied voltage to the two syringe needles (i.d. = 0.024 in.; Hamilton). The solution was supplied to the needle via two syringe pumps (Model NE-1000, New Era Pump Systems) and tubing (Pt. No. 30600-65, Cole Parmer). The entire set-up was contained in a box (dimensions = 16 in x 16 in x 28 in; Nalgene), which was continuously purged with dry air to maintain humidity at 5%.

The needle tip to collector distances, applied voltages, and solution flow rates were 7.5 and 9 cm, 7 and 12.5 kV, and 0.3 and 3 ml $h^{-1}$ for the electrospinning and electrospraying processes, respectively. The drum was rotated at 100 rpm, and the fiber mat was collected in the gap between the two magnets.

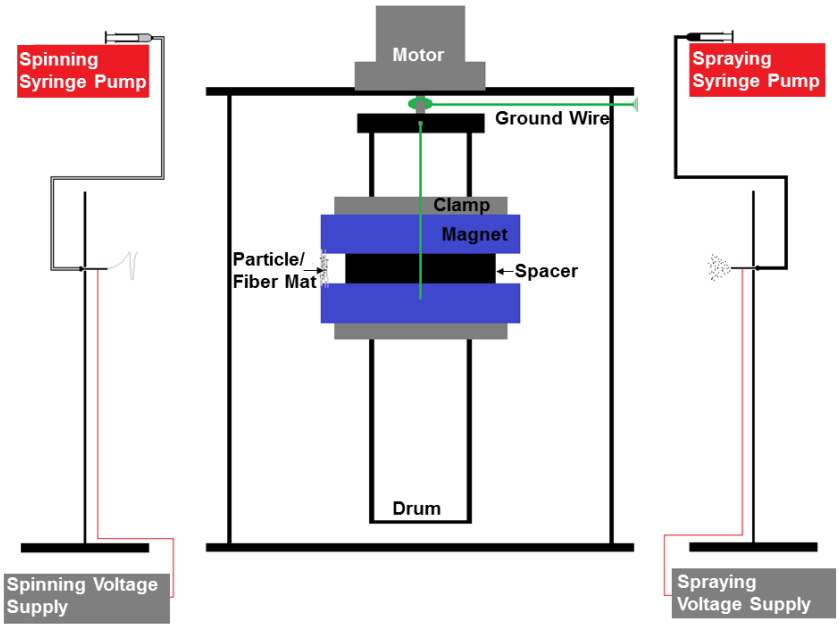


**Figure 2.1** Schematic of magnetic field apparatus.

### 2.2.5. Vertical Drum Apparatus

Figure 2.2 shows a schematic of the vertical drum apparatus developed. This apparatus was a modified version of the magnetic field apparatus in previous section. The magnets and PVC pipe were exchanged for a larger PVC pipe (o.d. = 4 in; McMaster-Carr) that was connected to the motor by a shaft. A strip of aluminum foil was used as the grounded collection surface. The motor, electrospinning and electrospraying apparatus, and

chamber were all used as described in previous section. The needle tip to collector distances, applied voltages, and solution flow rates were 7 and 9 cm, 6 and 12.5 kV, and 0.3 and 3 ml $h^{-1}$ for the electrospinning and electrospraying processes, respectively, with a drum rotation speed of 800 rpm.

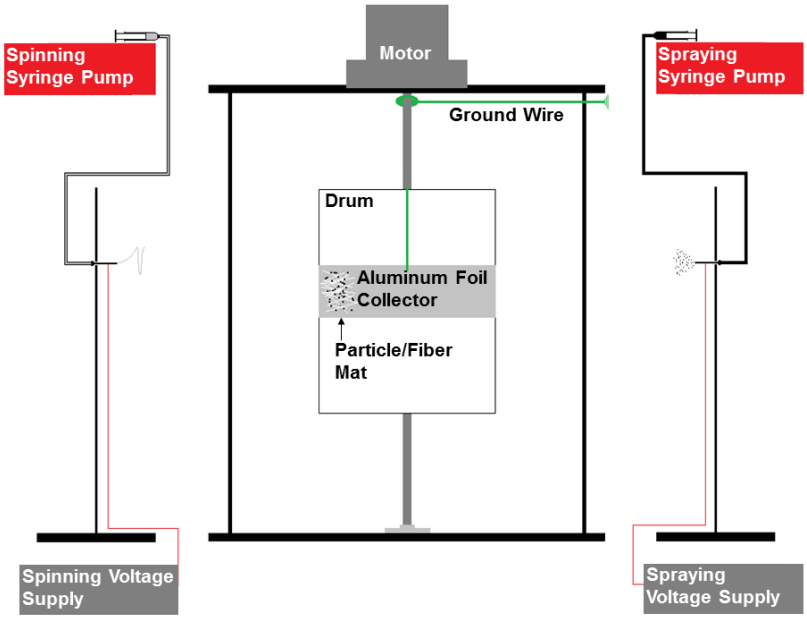


**Figure 2.2** Schematic of vertical drum apparatus.

### 2.2.6. Horizontal Drum Apparatus

A schematic of the horizontal drum apparatus developed is shown in Figure 2.3. The apparatus used a belt pulley as a drum (o.d. = 4 in, steel; 5706K11, McMaster-Carr), which was covered by grounded aluminum foil, not shown in the schematic, which served as the collection surface. The drum was powered by a motor (BMU5200APA3, Oriental Motor)

connected by a timing belt drive (gear ratio = 1.625; custom). The drum was mounted on a shaft (diameter = 0.5 in; 1570K42, McMaster-Carr) that was held in place by two ball bearings (cast iron; 7728T51, McMaster-Carr) that were mounted to a custom acetyl resin structure. The electrospinning and electrospraying apparatus and chamber were similar to previous sections. The needle tip to collector distances, applied voltages, and solution flow rates were 9 and 9 cm, 7 and 12.5 kV, and 1.0 and 3 ml $h^{-1}$ for the electrospinning and electrospraying processes, respectively, with a drum rotation speed of 6000 rpm.

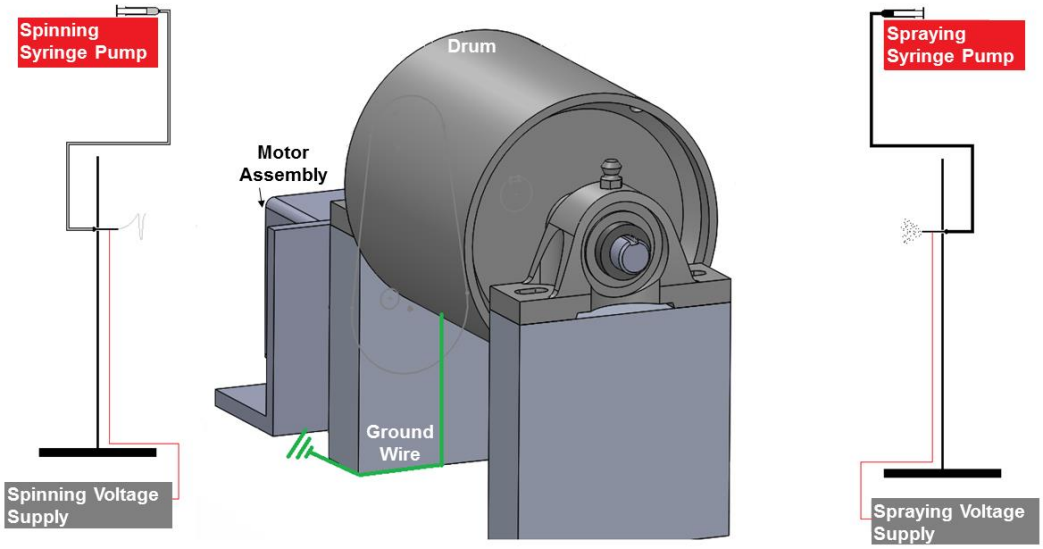


**Figure 2.3** Schematic of horizontal drum set-up.

## 2.3. Results and Discussion

### 2.3.1. Magnetic Field Apparatus

Several experiments were conducted using parallel ring magnets as described in the magnetic field apparatus experimental section. These experiments identified the spinning parameters required to reliably produce aligned fibers using this apparatus. It was observed that the needle to collection distance was most critical in fabricating an aligned fiber mat. These results are consistent with the findings reported by Rahmani *et al.*[30] Figure 2.4 (a) shows an SEM image of a fiber mat collected over 15 minutes under conditions described in the magnetic field apparatus experimental section. As shown in Figure 2.4 (b) shows, the sample is highly aligned and analysis of the histogram results in an alignment of 81%.

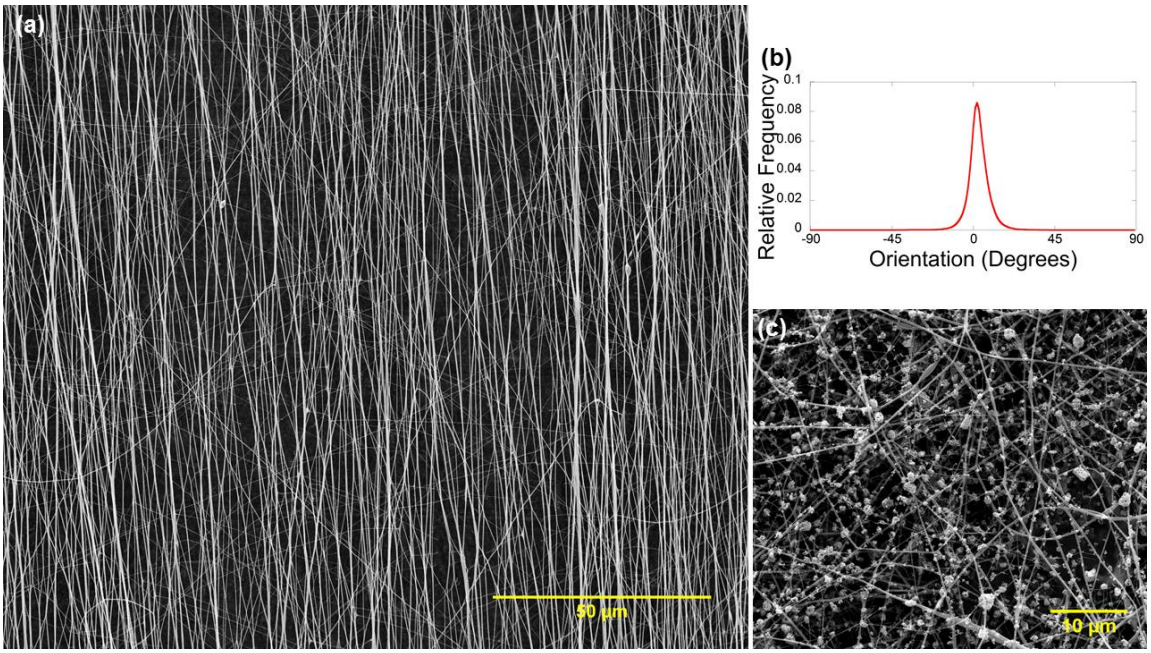


**Figure 2.4** (a) SEM image of fiber mat fabricated with magnetic field apparatus. (b) Orientation histogram. (c) SEM image of catalyst layer fabricated with magnetic field apparatus.

After successful fabrication of aligned fiber mats, attempts were made to produce similar alignments of the fiber mat while also spraying particles to create a complete catalyst layer. The introduction of electrospraying presented several challenges in the fabrication of catalyst layers. As Figure 2.4 (c) shows, the alignment results were not replicable once electrospraying was introduced. It was speculated that either physical or electrical interactions of the conducting particles were overcoming the aligning forces of the magnets. Additionally, Figure 2.5 shows a macroscopic picture of the resulting fiber mat. It is apparent that some of the electrospraying particles punctured through the relatively weak fiber mat. This was observed more frequently in the early stages of spinning before the mat reached a thickness such that the force of larger particles could be absorbed without puncturing. This resulted in mats having an inconsistent thickness and loading across the fiber mat.

**Figure 2.5** Photo of catalyst layer fabricated with magnetic field set-up.

In an attempt to create a catalyst layer without the interference of electrospraying, an electrospinning solution was made in a similar manner to the method reported by Zhang *et al*.[17] This electrospinning solution eliminated puncturing of the fiber mat, but did not result in an aligned mat. Figure 2.6 shows a SEM of the fiber mat made with the Pt/C electrospinning solution on the magnetic field apparatus. It is apparent that there is no to little alignment in this fiber mat. The addition of the Pt/C particles in the electrospinning solution makes the fibers very conductive. It seems the conductivity of either the spinning fiber or the collected mat affects the ability of the magnetic field to align the fibers.

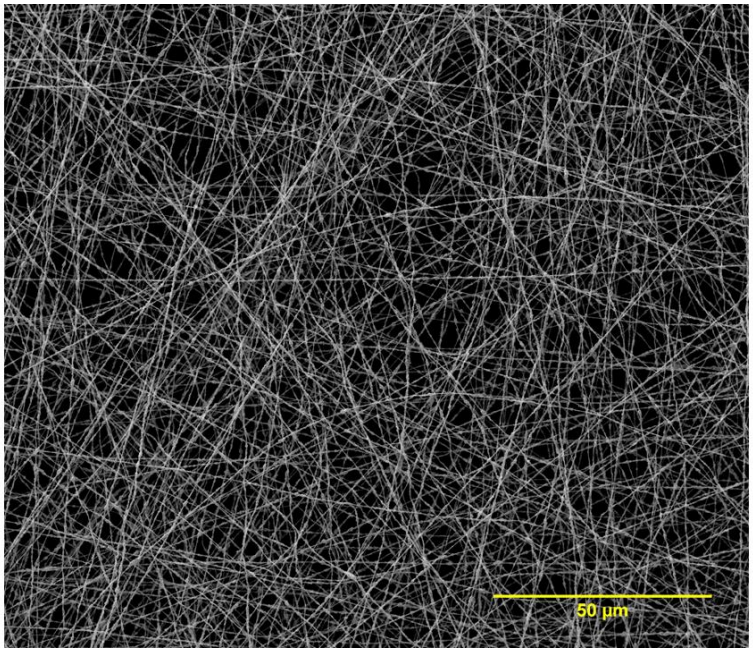


**Figure 2.6** SEM image of Pt/C spinning solution fiber mat fabricated with magnetic field apparatus.

### 2.3.2. Accelerated Drum Apparatus

Figure 2.7 (a) shows the fiber mat collected on the vertical drum apparatus. While it is clear there is a tendency for alignment, the overall alignment percentage is 71%, which is lower than the alignment achieved by the magnetic field apparatus. Figure 2.7 (c) shows that the introduction of the spraying technique does not affect the alignment of the fibers in the catalyst layer.

Figure 2.8 (a) shows a fiber mat, which was produced on the horizontal drum apparatus. It is apparent that the alignment increases significantly with the increased face velocity of the drum over the vertical drum configuration. This observation is confirmed by image analysis, which gives the alignment percentage of the fibers at 80%, similar to that obtained in magnetic field electrospinning. The horizontal drum is a more stable apparatus than the vertical drum with an improved motor, which allows for a faster drum speeds. This higher speed enables the spinning fiber to be subject to higher aligning forces when making contact with the collection surface, resulting in a fiber mat with a higher alignment.

(a) SEM image of fiber mat fabricated with vertical drum apparatus. (b) Orientation histogram. (c) SEM image of catalyst layer fabricated with vertical drum apparatus. (a) SEM image of fiber mat fabricated with horizontal drum apparatus. (b) Orientation histogram. (c) SEM image of catalyst layer fabricated with horizontal drum apparatus.

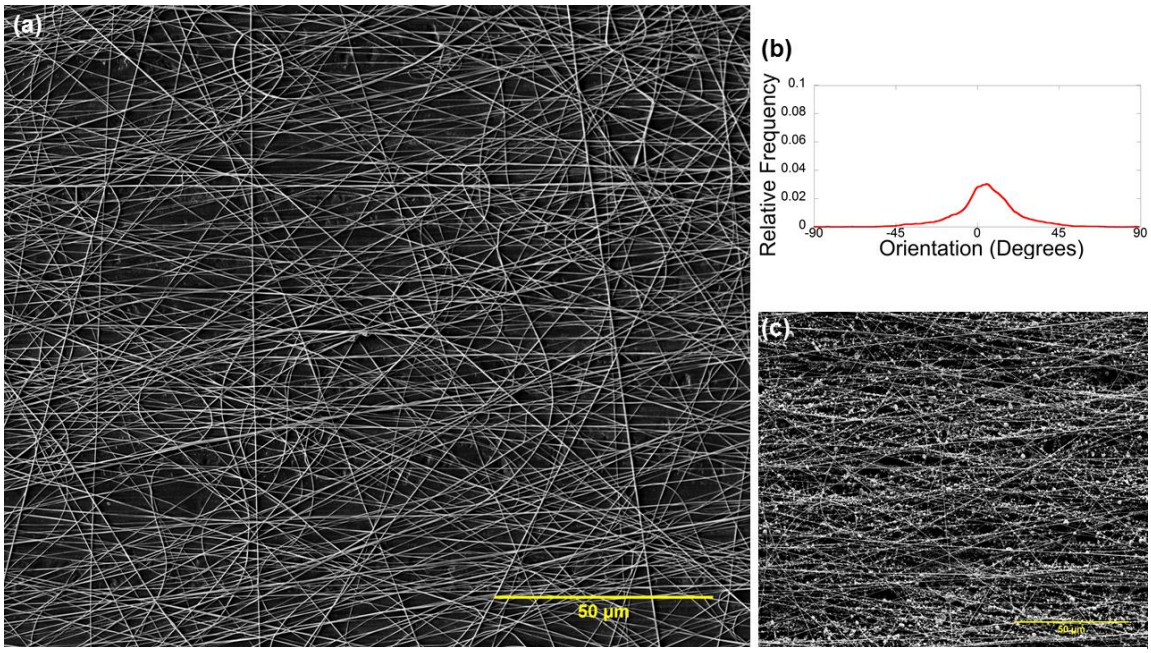


**Figure 2.7** (a) SEM image of fiber mat fabricated with vertical drum apparatus. (b) Orientation histogram. (c) SEM image of catalyst layer fabricated with vertical drum apparatus.

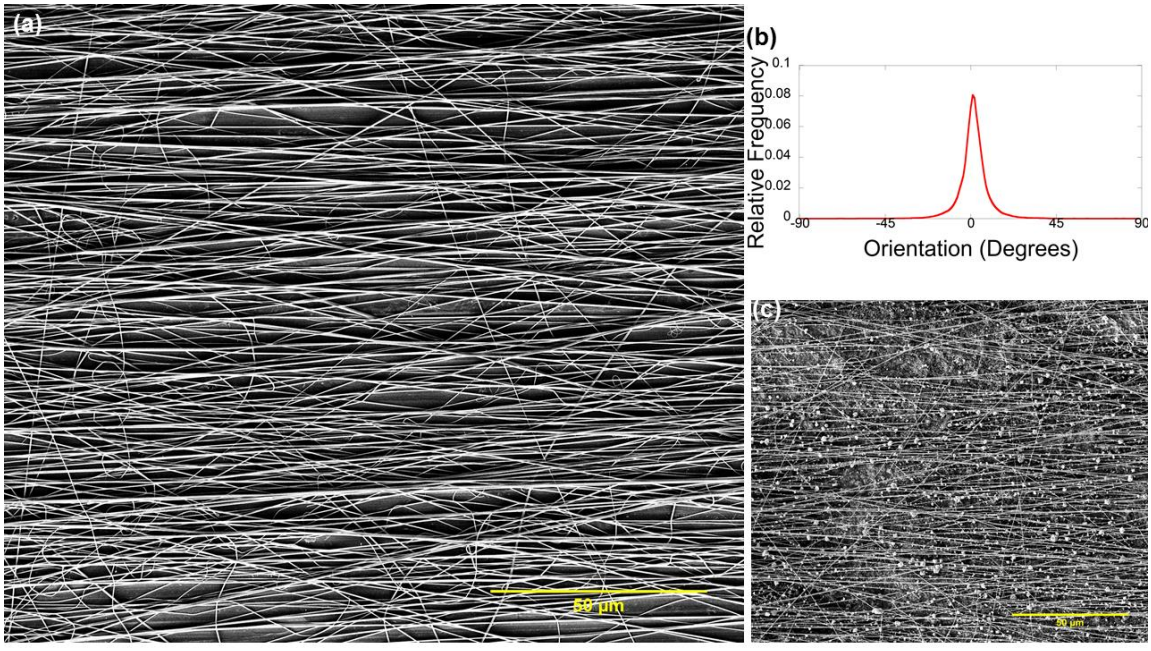


**Figure 2.8** (a) SEM image of fiber mat fabricated with horizontal drum apparatus. (b) Orientation histogram. (c) SEM image of catalyst layer fabricated with horizontal drum apparatus.

## 2.4. Conclusion

In this section, the horizontal drum apparatus demonstrates the ability to fabricate a highly aligned fiber mat and catalyst layer. The magnetic field apparatus, while able to produce an aligned fiber mat, was unable to fabricate an aligned catalyst layer. Future studies will further explore orientation using the horizontal drum and the fuel cell performance of the aligned catalyst layers. The vertical drum apparatus produces an aligned fiber mat and catalyst layer, but the alignment was not as high as observed with the magnetic field apparatus or horizontal drum apparatus.

# 3. ALIGNED NAFION FIBER MATS ON ACCELERATED DRUM

## 3.1. Introduction

The goal of this study is to explore the range of alignments possible on the accelerated drum apparatus developed in the previous section. There are many parameters, which can be tailored in electrospinning, such as needle to collector distance, strength of the electric field, temperature, humidity, solution flow rate, and drum speed. In this section, drum speed and solution flow rate were varied and the effects on the spinning process and orientation are reported.

## 3.2. Experimental Methods

### 3.2.1. Materials

Isopropanol (99.5%, Sigma Aldrich), Nafion solution (1100 EW, 5 wt% in a 3/1 v/v of isopropanol/water, Ion Power), and poly(acrylic acid) (PAA; $M_V$ = 450,000 g $mol^{-1}$, Sigma Aldrich) were used as received. Ultrapure deionized (DI) with resistivity greater than 16 MΩ·cm (25 °C) was used as appropriate.

### 3.2.2. Fiber Characterization

Scanning electron microscopy (SEM; FEI Quanta 600 FE-SEM; 5 kV; working distance = 10 cm) was used to investigate the morphology of the fibers. The samples were

removed from the collector after spinning. Samples were sputter coated (Cressington 208 HR) with platinum/palladium (thickness = 10 nm).

Image analysis was performed using ImageJ software to characterize the fiber diameter and orientation. DiameterJ was used to segment the image and calculate the diameter of the fibers. OrientationJ was utilized to obtain the orientation distribution of the fibers. This distribution was converted to an overall percentage *via* the method reported by Rahmani *et al.*[30] This method uses the relative frequencies in the histogram and weighs them based on the distance from the target orientation. This method will assign a value of 100% aligned to a sample completely aligned in the target direction, 0% aligned to a sample completely aligned perpendicular to the target direction, and 33% aligned to a sample with completely random alignment. In this work, the target direction was always chosen as the orientation, which provided the best fit of the histogram to a normal curve.

### 3.2.3. Preparation of Electrospinning Solution

The electrospinning solution used for the creation of fiber mats was fabricated with the following specifications. 18.75 mg of PAA, 1500 mg of Nafion solution, and 375 mg of isopropanol/water (3/1 v/v) were added to obtain a 5% by weight in the polymer solution. The resulting solution contained a 4/1 w/w Nafion/PAA ratio. The solution was allowed to stir for several hours until PAA was completely dissolved.

### 3.2.4. Electrospinning Apparatus

A schematic of the horizontal drum apparatus developed is shown in Figure 3.1. The apparatus used a belt pulley as a drum (o.d. = 4 in, steel; 5706K11, McMaster-Carr), which was covered by grounded aluminum foil, not shown in the schematic, which served as the collection surface. The drum was powered by a motor (BMU5200APA3, Oriental Motor) connected by a timing belt drive (gear ratio = 1.625; custom). The drum was mounted on a shaft (diameter = 0.5 in; 1570K42, McMaster-Carr) that was held in place by two ball bearings (cast iron; 7728T51, McMaster-Carr) that were mounted to a custom acetyl resin structure. The assembly was driven by a motor (Model 4IK25GN-SW2, Oriental Motor). On either side of the assembly, a high-voltage power supply (Model PS/EL50R00.8, Glassman High Voltage, Inc.) supplied voltage to the syringe needle (i.d. = 0.024 in.; Hamilton). The solution was supplied to the needle *via* a syringe pump (Model NE-1000, New Era Pump Systems) and tubing (Pt. No. 30600-65, Cole Parmer). The entire apparatus was contained in a box (dimensions = 16 in x 16 in x 28 in; Nalgene), which was continuously purged with dry air to maintain humidity at 5%. The needle tip to collector distance and applied voltage is 9 cm and 7 kV, respectively. The flow rate was varied between 0.1 and 1.0 ml $h^{-1}$ and the drum rotation speed was varied from 1000 to 6000 rpm during the experiments. Collection times were varied to maintain a similar fiber mat thickness between experiments. The times used were 10, 13, 20, 30, and 30 minutes for the 1.0, 0.75, 0.5, 0.3, and 0.1 ml $h^{-1}$ flow rates, respectively.

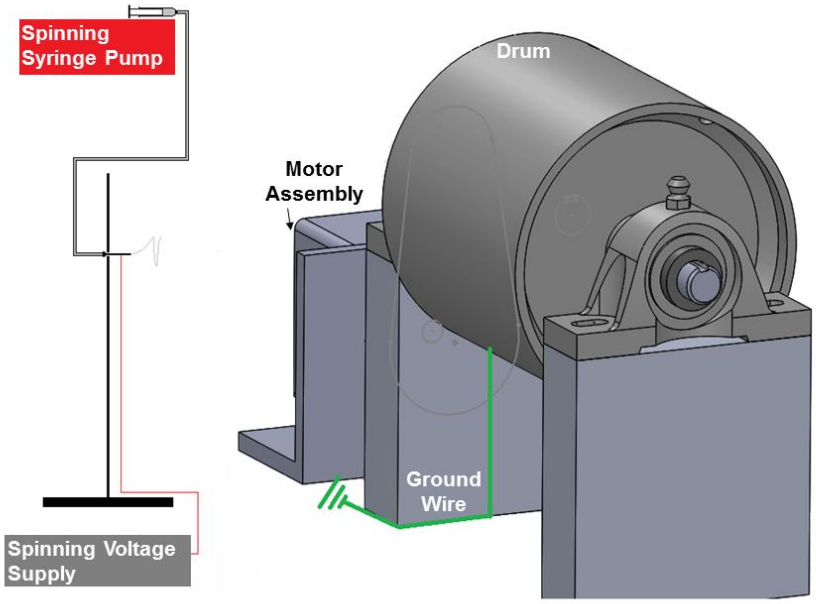


**Figure 3.1** Schematic of electrospinning apparatus.

### 3.3. Results and Discussion

Figure 3.2 shows the results of operating the electrospinning apparatus at 0.1 ml $h^{-1}$ at drum speeds ranging from 1000 to 5000 rpm. The low flow rate introduced several challenges. The primary difficulty was maintaining a stable spinning jet since the low flow rate would often result in oscillation of the Taylor cone formation and solution buildup at the tip. Also, occasional solution drying at the tip was observed. The SEM images show that very few fibers were collected, especially relative to the higher flow rates at the higher rpms. This is partially due to the lower collection time relative to the flow rate, but the number of fibers collected also decreases with increasing drum speed. This could be a

result of the air movement surrounding the drum increasing as a function of drum speed. Combined with the unstable jet, the high air velocities may have deterred the fibers from collecting on the collection surface. Another explanation is the fiber breaking at higher drum speeds. If the physical force that the rotating drum exerts on the fiber is too high, the fiber can stretch and break. Figure 3.2 (d) shows a clear example of a broken fiber near the top of the image. Having fewer fibers to analyze affects the orientation results since error is expected to increase with the lowered sample size.

The graph of alignment shows that overall the orientation trends up with drum speed. There is a potential outlier at 2000 rpm. It is suspected that this is a result of both lower fiber count and an unusually highly orientated site where the SEM was taken since other results do not contain such an outlier; however, more investigation is needed to confirm this. Excluding this outlier from the analysis shows a clear correlation between fiber diameter and drum speed. The alignment of the samples ranges from 70% to 77%.

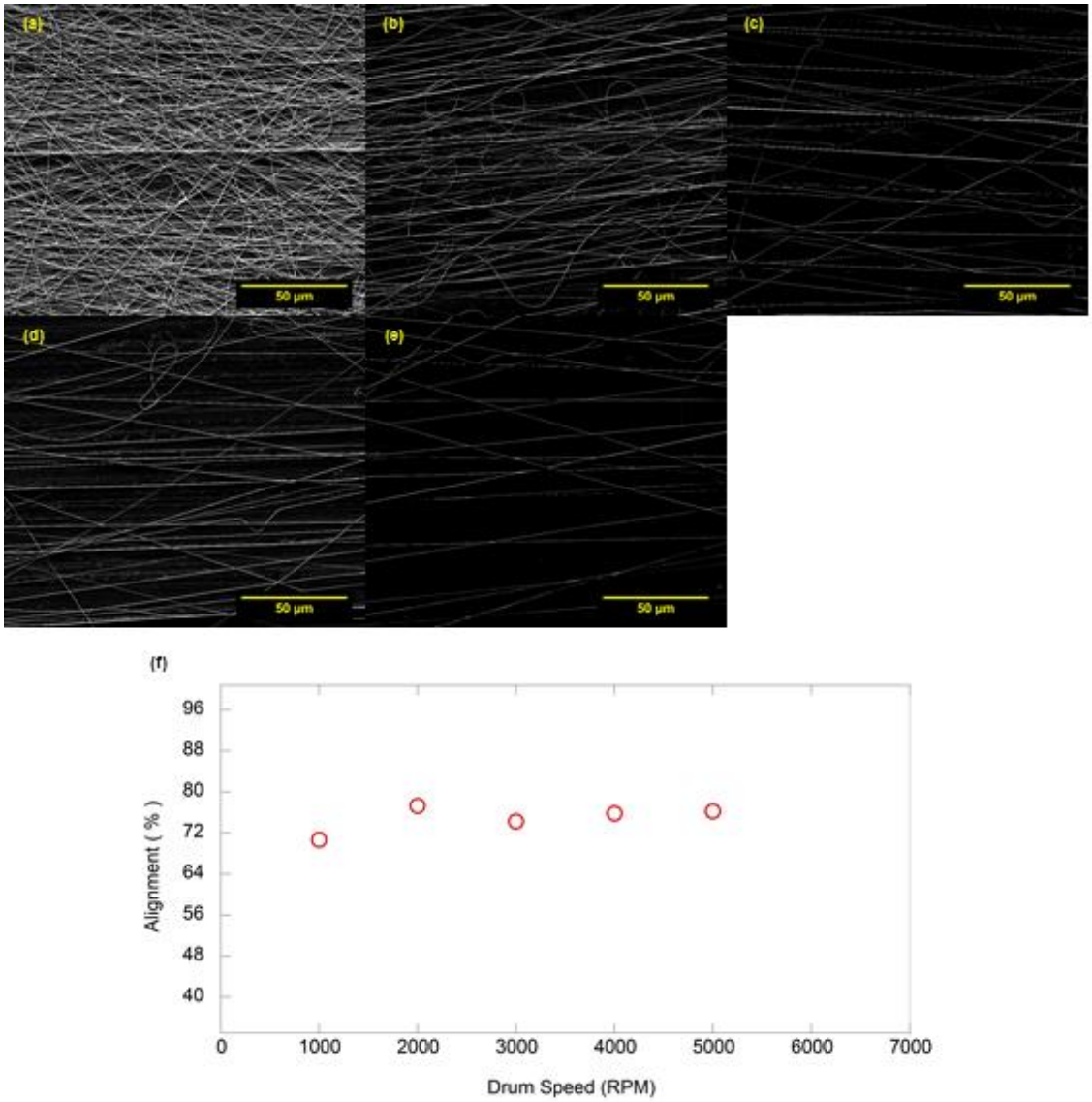


**Figure 3.2** SEM images of fiber mats with flow rate of 0.1 ml h-1 and drum speed of (a) 1000, (b) 2000, (c) 3000, (d) 4000, and (e) 5000 rpm. (f) Graph of alignment percentage for shown SEMs.

Figures 3.3 and 3.4 show the results for 0.3 and 0.5 ml $h^{-1}$, respectively. These flow rates were far easier to spin than the 0.1 ml $h^{-1}$, but the instability did increase at higher drum speeds. This did not seem to affect the collection or alignment of fibers significantly since instability was observed at 4000 rpm, which is also the peak alignment. The

alignment trend does increase as expected from ~70% to ~80%, but sees a decline at 5000 rpm to 77%. The SEM images reveal several broken fibers in both the 0.3 and 0.5 ml $h^{-1}$ 5000 rpm fiber mats. This breakage causes a visual decrease in the number of fibers collected and a slight reduction of the overall alignment of the fiber mat.

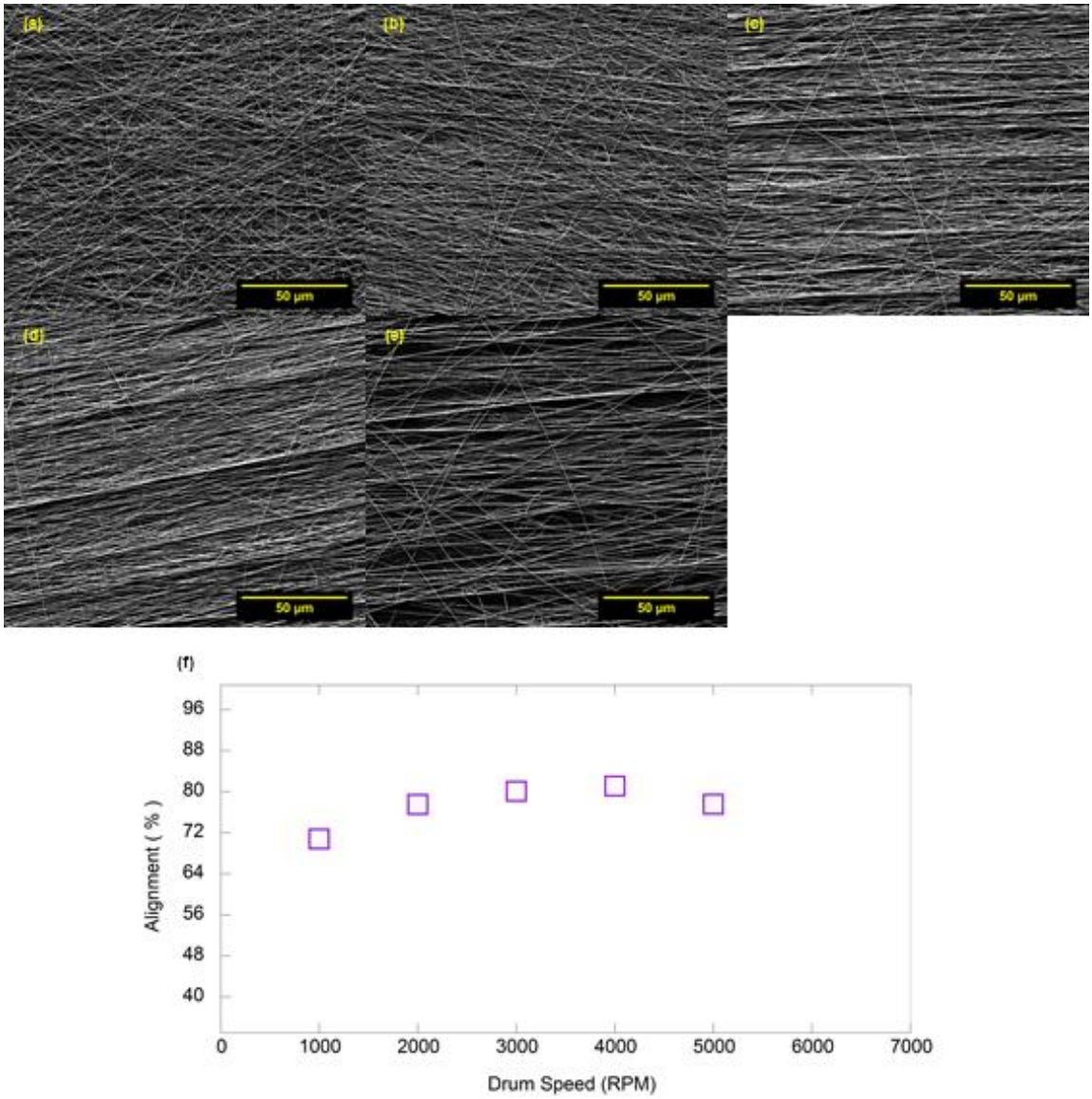


**Figure 3.3** SEM images of fiber mats with flow rate of 0.3 ml h-1 and drum speed of (a) 1000, (b) 2000, (c) 3000, (d) 4000, and (e) 5000 rpm. (f) Graph of alignment percentage for shown SEMs.

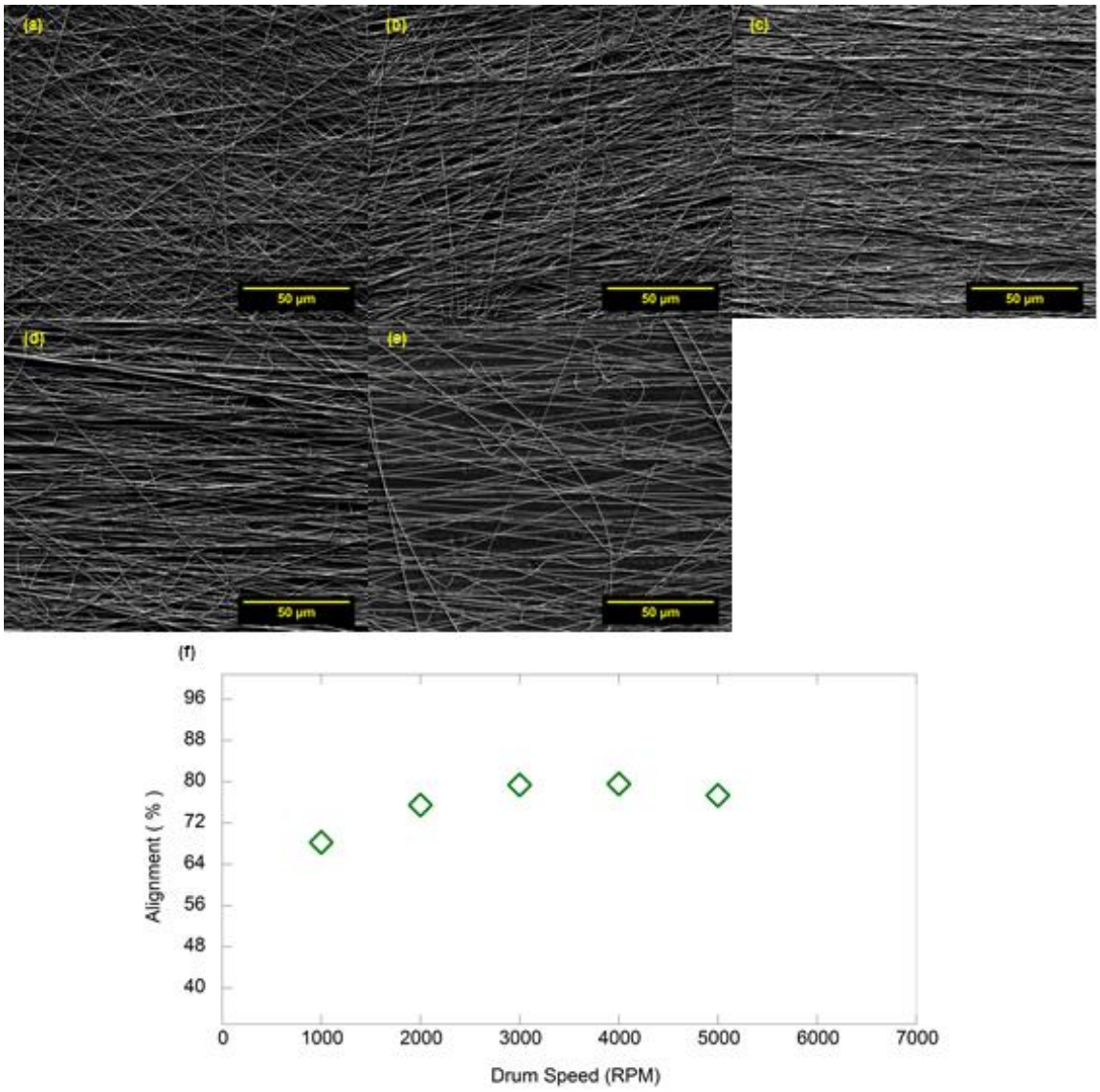


**Figure 3.4** SEM images of fiber mats with flow rate of 0.5 ml h-1 and drum speed of (a) 1000, (b) 2000, (c) 3000, (d) 4000, and (e) 5000 rpm. (f) Graph of alignment percentage for shown SEMs.

The results of 0.75 and 1.0 ml $h^{-1}$ flow rates are given in Figures 3.5 and 3.6, respectively. Both of these flow rates show an increase in alignment with increasing rpm that begins to plateau at 4000 rpm around 80% alignment. While spinning, both of these flow rates were extremely stable even at the higher drum speeds. Broken fibers, reduction

of alignment percentage, and decrease in fiber collection were not observed in any of the SEM images at all drum speeds.

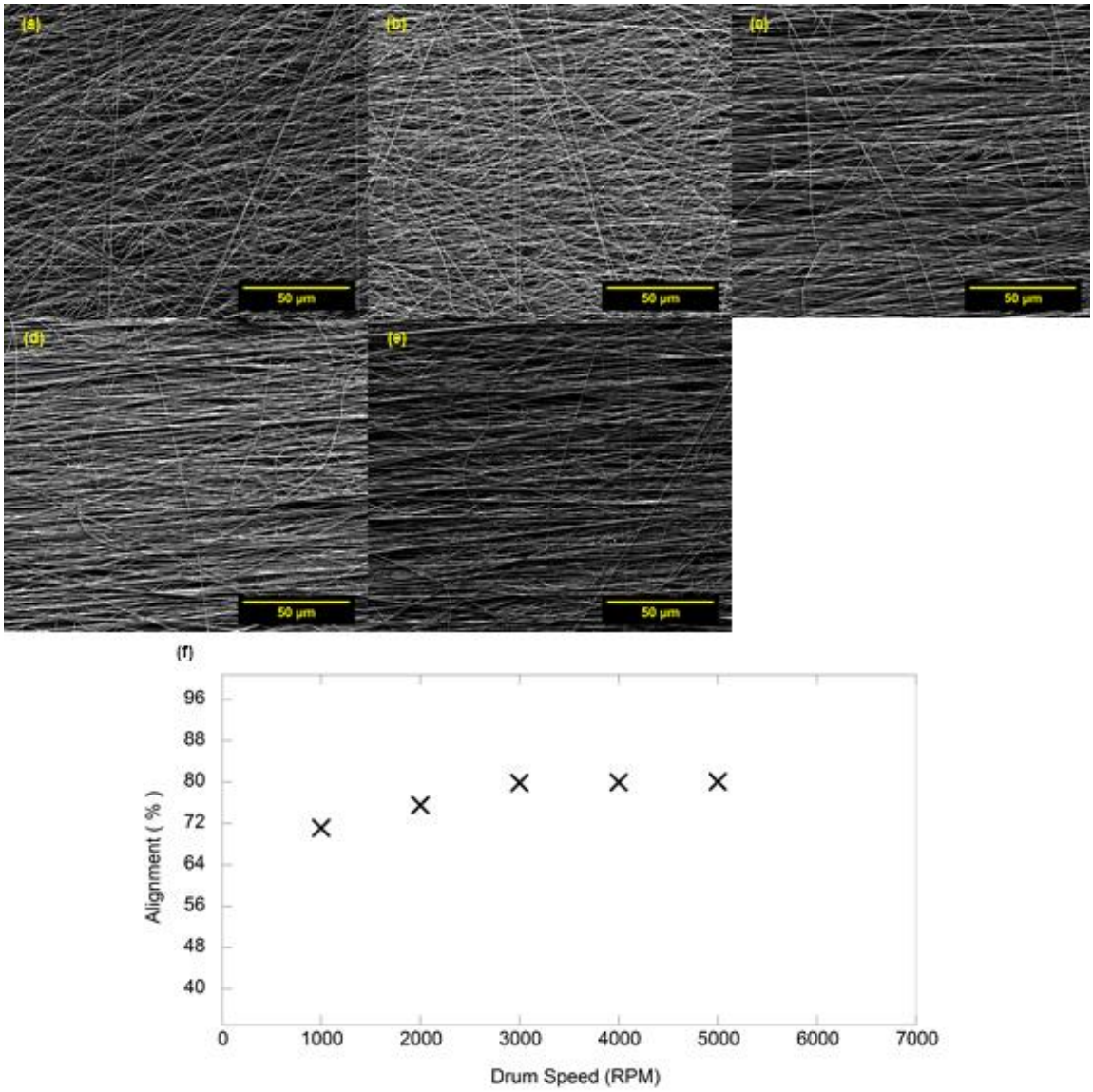


**Figure 3.5** SEM images of fiber mats with flow rate of 0.75 ml h-1 and drum speed of (a) 1000, (b) 2000, (c) 3000, (d) 4000, and (e) 5000 rpm. (f) Graph of alignment percentage for shown SEMs.

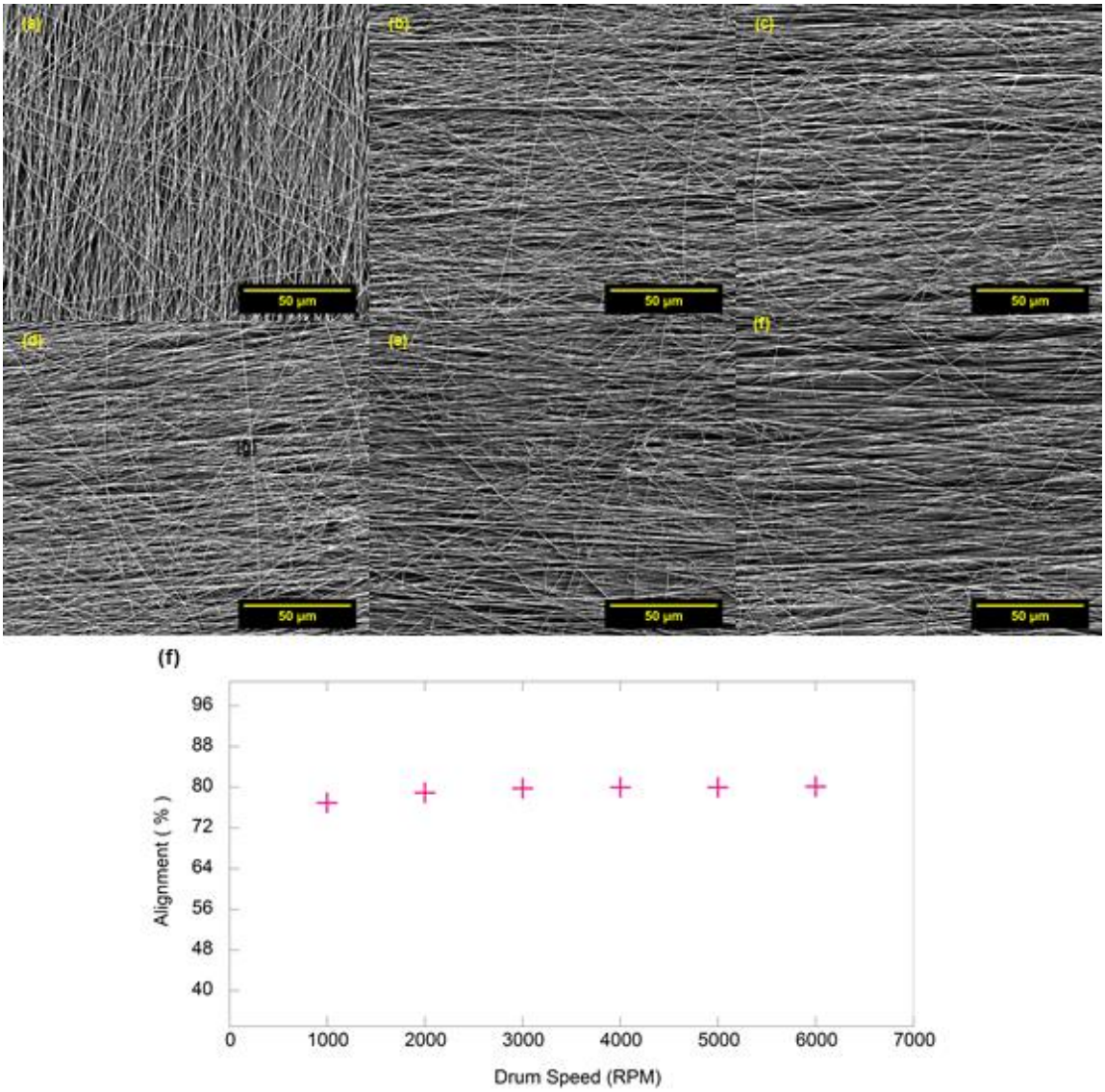


**Figure 3.6** SEM images of fiber mats with flow rate of 1.0 ml h-1 and drum speed of (a) 1000, (b) 2000, (c) 3000, (d) 4000, (e) 5000 rpm, and (f) 6000 rpm. (f) Graph of alignment percentage for shown SEMs.

Figure 3.7 compares all of the flow rates on one graph. The graph shows that there is a definite trend of alignment with rpm, but it does not show a clear trend of alignment with flow rate. This allows for selection of flow rate to be made based on other considerations, such as ease of spinning and likelihood of broken fibers. In all cases, but 0.1 ml $h^{-1}$, the

maximum alignment was approximately 80%. Also, worth considering is the fiber breakage observed in the lower flowrates that causes a reduction in the fibers collected and overall alignment past approximately 4000 rpm. Fiber diameter has a role in the conductivity of Nafion.[31] Therefore, it is critical to determine whether the spinning conditions have an effect on the average fiber diameter. Figure 3.8 shows that the average fiber diameter is consistently in the 300-400 nm range. The only exception is higher drum speeds at 0.1 ml $h^{-1}$ flow rate. This is most likely due to the previously mentioned fiber stretching and breaking at the higher speeds.

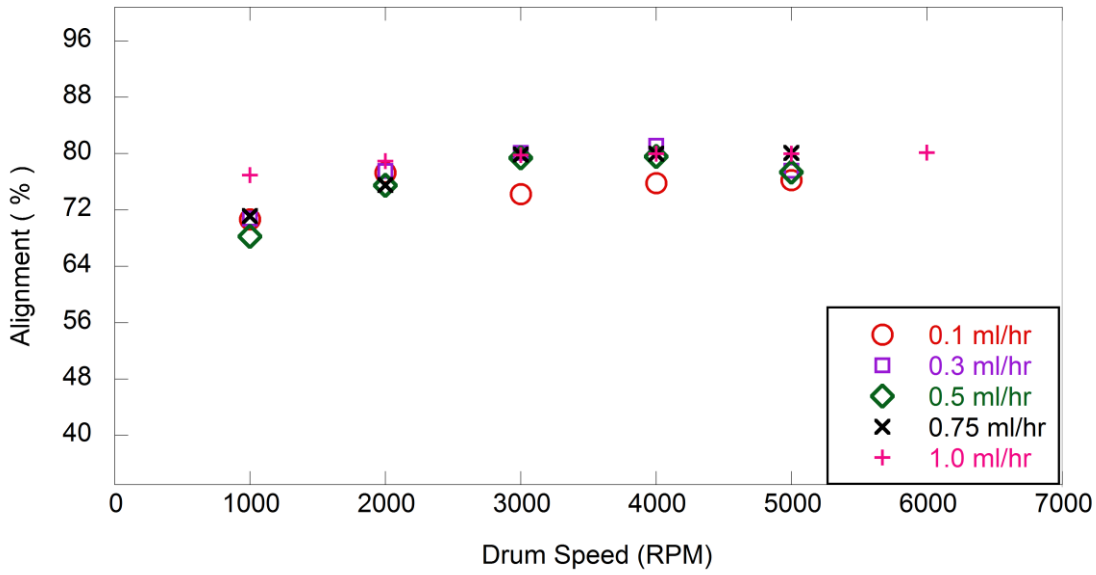


**Figure 3.7** Fiber alignment percentage of 0.1 (red), 0.3 (purple), 0.5 (green), 0.75 (black), and 1.0 (pink) ml h-1 flow rates at varying drum speeds.

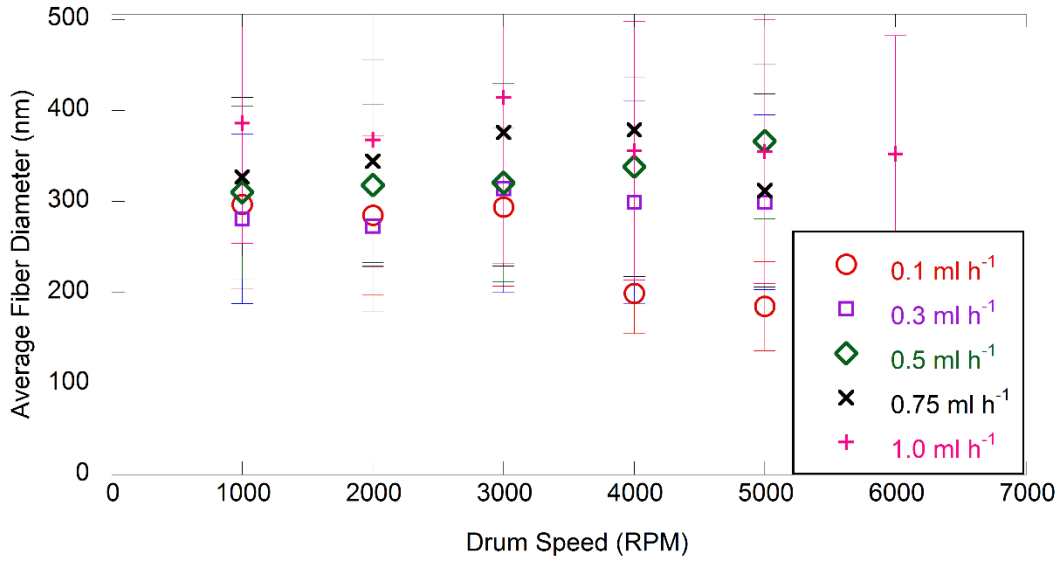


**Figure 3.8** Average fiber diameters of 0.1 (red), 0.3 (purple), 0.5 (green), 0.75 (black), and 1.0 (pink) ml h-1 flow rates at varying drum speeds. Error bars show standard deviation.

## 3.4. Conclusions

In this study, a range of flow rates from 0.1 - 1.0 ml $h^{-1}$ and drum speeds from 1000 – 6000 rpm were explored to determine the effect these parameters had on the fabrication of an aligned fiber mat. Alignment was demonstrated to be a function of drum rotation speed with the upper limit approaching 80% alignment in this setup. Solution flow rate was not a strong indicator of alignment, but did affect the spinning characteristics. Higher flow rates reduced or eliminated fiber breakage that was observed in lower flow rates. Fiber diameter was also found to be insignificantly affected by the parameters.

# 4. FUEL CELL PERFORMANCE OF ALIGNED CATALYST LAYER

## 4.1. Introduction

In this study, the alignment achieved in previous chapters is applied to the fabrication of a fuel cell catalyst layer. The effects of the fiber alignment on the morphology of the catalyst layer and performance of the membrane electrode assembly (MEA) in a fuel cell is compared to a control with random fibers. The performance is compared on the basis of peak power and electrochemical surface area (ECSA), which corresponds to the overall performance capabilities of the cell and the number of TPBs, respectively.

## 4.2. Experimental Methods

### 4.2.1. Materials

Isopropanol (99.5%, Sigma Aldrich), Nafion solution (1100 EW, 5 wt% in a 3:1 v:v of isopropanol/water, Ion Power), poly(acrylic acid) (PAA; MV = 450,000 g $mol^{-1}$, Sigma Aldrich), 20 wt% platinum on carbon catalyst (Pt/C; Vulcan XC-72, Premetek Co.), gas diffusion layer (GDL; SGL-25BC; Fuel Cells Etc.), and Nafion NR-212 membrane (1100 EW, dry thickness = 50 mm; Ion Power) were used as received. Ultrapure deionized (DI) with resistivity greater than 16 MΩ cm (25 °C) was used as appropriate. Ultra high purity grade $N_2$ was purchased from Brazos Valley Welding Supply. Ultra high purity grade $O_2$ was purchased from Airgas. Ultra high purity grade $H_2$ was purchased from Praxair.

### 4.2.2. Electrode Characterization

*SEM*

Scanning electron microscopy (SEM; FEI Quanta 600 FE-SEM; 5 kV; working distance = 10 cm) was used to investigate the morphology of the fibers. The samples were removed from the collector after spinning. Samples were sputter coated (Cressington 208 HR) with platinum/palladium (thickness = 10 nm).

*Surface Porosity*

Image analysis was performed using ImageJ software to characterize the 2D projection of porosity in the SEM images. DiameterJ was used to segment the image and measure the area of the individual pores and get an overall porous area of the image.

*Thermal Gravimetry Analysis (TGA)*

Platinum loading was measured by pyrolyizing the electrode with thermal gravimeteric analysis (TGA; Q50; TA Instrument) on a 5 mg sample of the electrode. The procedure used ramped the temperature from 25 °C to 900 °C at a rate of 10 °C/min in the presence of an air flowing at 20 mL/min. At 900 °C, the only component of the electrode remaining is platinum; therefore, the final weight of the experiment was used to calculate platinum loading.

### 4.2.3. Preparation of Solutions

The electrospinning solution used for the creation of fiber mats was fabricated with the following specifications. 18.75 mg of PAA, 1500 mg of Nafion solution, and 375 mg of isopropanol/water (3/1 v/v) were added to obtain a 5% by weight in the polymer solution.

The resulting solution contained a 4/1 w/w Nafion/PAA ratio. The solution was allowed to stir for several hours until PAA was completely dissolved.

The electrospraying solution was fabricated by adding 40 mg of 20% Pt/C, 32 mg of Nafion at 5% of the carbon weight, and 3.9 g isopropanol/water (3/1 v/v) to reach 1% solids in the solution. The solution was then sonicated (duration = 5 min, amplitude = 35%; Model CL-18, Qsonica Sonicator) to disperse the Pt/C.

### 4.2.4. Electrospinning Apparatus

A schematic of the horizontal drum apparatus developed is shown in Figure 4.1. The apparatus used a belt pulley as a drum (o.d. = 4 in, steel; 5706K11, McMaster-Carr), which was covered by grounded aluminum foil, not shown in the schematic, which served as the collection surface. The drum was powered by a motor (BMU5200APA3, Oriental Motor) connected by a timing belt drive (gear ratio = 1.625; custom). The drum was mounted on a shaft (diameter = 0.5 in; 1570K42, McMaster-Carr) that was held in place by two ball bearings (cast iron; 7728T51, McMaster-Carr) that were mounted to a custom acetyl resin structure. The assembly was driven by a motor (Model 4IK25GN-SW2, Oriental Motor). On either side of the assembly, high-voltage power supplies (Model PS/EL50R00.8, Glassman High Voltage, Inc.) supplied voltage to the syringe needles (i.d. = 0.024 in.; Hamilton). The solution was supplied to the needles *via* a syringe pump (Model NE-1000, New Era Pump Systems) and tubing (Pt. No. 30600-65, Cole Parmer). The entire apparatus was contained in a box (dimensions = 16 in x 16 in x 28 in; Nalgene) that was continuously purged with dry air to maintain humidity at 5%.

The needle tip to collector distance, applied voltage, and flow rate were 9 cm, 7 kV, 0.75 ml $h^{-1}$, respectively for electrospinning. For electrospraying, the needle tip to collector distance, applied voltage, and flow rate were 9 cm, 12 kV, 5 ml $h^{-1}$, respectively. The drum rotation speed was 100 RPM for the control experiment and 4000 rpm for the aligned experiment. The collection was stopped once the spraying solution was consumed.

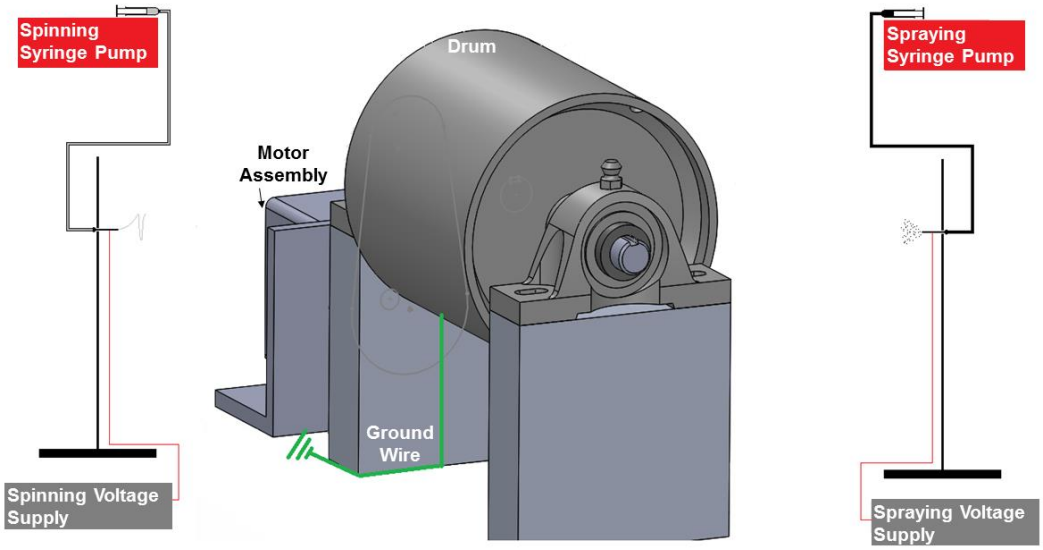


**Figure 4.1** Schematic of electrospinning and electrospraying apparatus.

The catalyst layers were prepared by applying the GDL, cut into 2 cm x 3 cm rectangles, to the aluminum foil on the steel drum. The apparatus was then used to coat the GDL in a fiber and catalyst particle mat to form an electrode. This large electrode was cut to 1.1 cm x 1.1 cm squares to form both the anode and cathode electrodes. The Nafion NR-212

membrane was sandwiched by the anode and cathode electrodes and hot pressed (heat press, Carver) at a temperature of 275 °F and pressure of 1300 psi for 5 minutes.

### 4.2.5. Characterization of MEAs

*Fuel Cell*

The MEAs were tested in a fuel cell test station (850C; Scribner Associates, Inc). The fuel cell assembly consists of MEA (area = 1.21cm$^2$) centered between two Teflon gaskets (0.006" thick; Scribner Associates, Inc), graphite plates with a 1 cm$^2$ serpentine flow channel, copper plates, and aluminum end plates. The end plates were bolted together with each bolt torqued to 100 lb in of torque. The fuel cell conditions were held at ambient pressure and 80 °C for the duration of activation and performance testing. The fuel flow rate was 0.42 L min$^{-1}$ of $H_2$ and 1 L min$^{-1}$ of $O_2$ at 80 °C and 100% relative humidity.

The activation procedure held the fuel cell at 0.7 V for 1 hour followed by holding at 0.6 V and 0.4 V for 30 minutes each. The 0.6 V and 0.4 V holds were repeated twice for a total activation period of 4 hours. The performance test began at the open circuit voltage and terminated at 0.2 V. The current was recorded every 0.05 V after allowing the current to stabilize for 1 minute.

*Cyclic Voltammetry (CV) and Electrochemical Surface Area (ECSA)*

A potentiostat (Solartron SI 1287, Corrware Software) was used to perform CV tests on the MEA. The tests were performed at ambient pressure and 30 °C with a fuel flow rate of 0.04 L min$^{-1}$ $H_2$ in the anode and 0.02 L min$^{-1}$ $N_2$ in the cathode. The MEA was cycled from 0.05 V to 1 V at 20 mV/s for 5 cycles. The Pt catalyst was assumed to have an

average site density of 210 mC $cm^{-1}$. The electrochemical surface area (ECSA) was determined from the hydrogen adsorption area from 0.1 to 0.4 V of the CV data.

## 4.3. Results and Discussion

The catalyst layers were made *via* the methods given above. Figure 4.2 shows SEM images of both the aligned and control catalyst layers. These images show that the aligned catalyst layer has few fibers that vary more than a few degrees from the primary direction of alignment. Due to the presence of the catalyst particles, the alignment could not be quantified in a similar manner to previous chapters; however, these spinning conditions resulted in an alignment of ~80% previously. Visually, the surface porosity appears similar between the aligned and control catalyst layer. This is confirmed by the similar percentage porosity given in the DiameterJ analysis of Figure 4.2 (b) and (e) with the aligned layer 56% porous and the control image 53% porous. This suggests that the gas transport, which is dependent on the porosity, should be similar between the aligned and control layers. The aligned catalyst layer shows large areas of agglomeration on the order of 100 – 300 µm compared to the agglomerations ranging from ~50 – 150 µm. Because these agglomerations have minimal porosity, gas transport resistance is increased, causing a reduction in performance at higher currents.

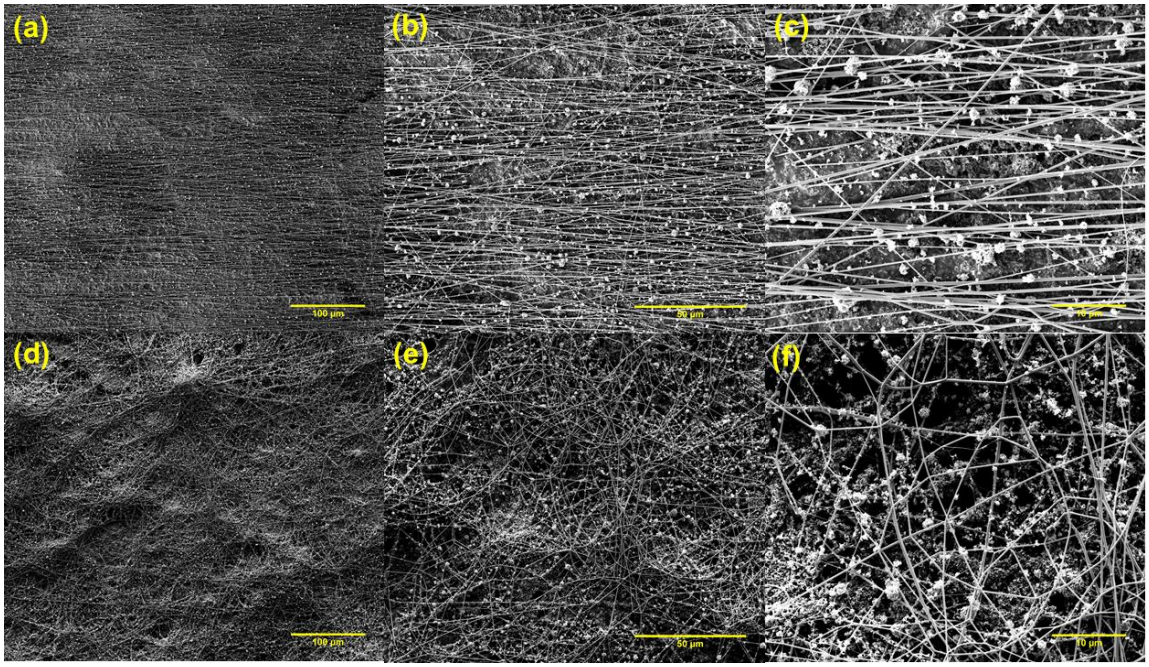


**Figure 4.2** SEM images of the aligned catalyst layer at (a) 500, (b) 1500, and (c) 5000 times magnification and control catalyst layer at (d) 500, (e) 1500, and (f) 5000 times magnification.

The resulting platinum loading was 0.060 $mg_{Pt}$ $cm^{-2}$ in the aligned cathode and 0.074 $mg_{Pt}$ $cm^{-2}$ in the control cathode. In Figure 4.3 (a), it is shown that the aligned MEA has a peak power density of 530 mW $cm^{-2}$ at a voltage of 346 mV, which is steady over 4 separate runs. Figure 4.3 (b) shows that the control is also at steady state with a peak power density of 535 mW $cm^{-2}$ at 342 mV. In Figure 4.4, the performance of the aligned catalyst layer is shown to be similar to the control with a nearly identical peak power density. Interestingly, the aligned MEA begins to show mass transport losses at ~1800 mA $cm^{-2}$, sooner than control which begins to drop at ~2400 mA $cm^{-2}$. This is likely due to the larger agglomerates previously seen in the SEM images. Also shown are the CV results, which were used to analyze the ESCA, which was found to be 42 $m^2$ $g_{Pt}^{-1}$ for the control MEA and 43 $m^2$ $g_{Pt}^{-1}$ for the aligned MEA.

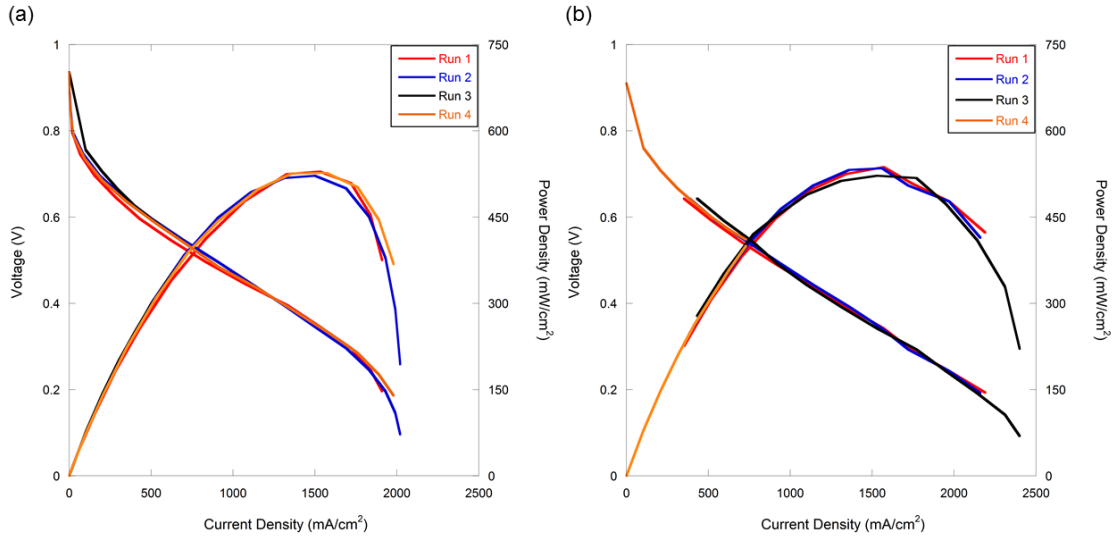


**Figure 4.3** Fuel cell performance curves of the (a) aligned fiber catalyst layer and (b) random fiber control catalyst layer.

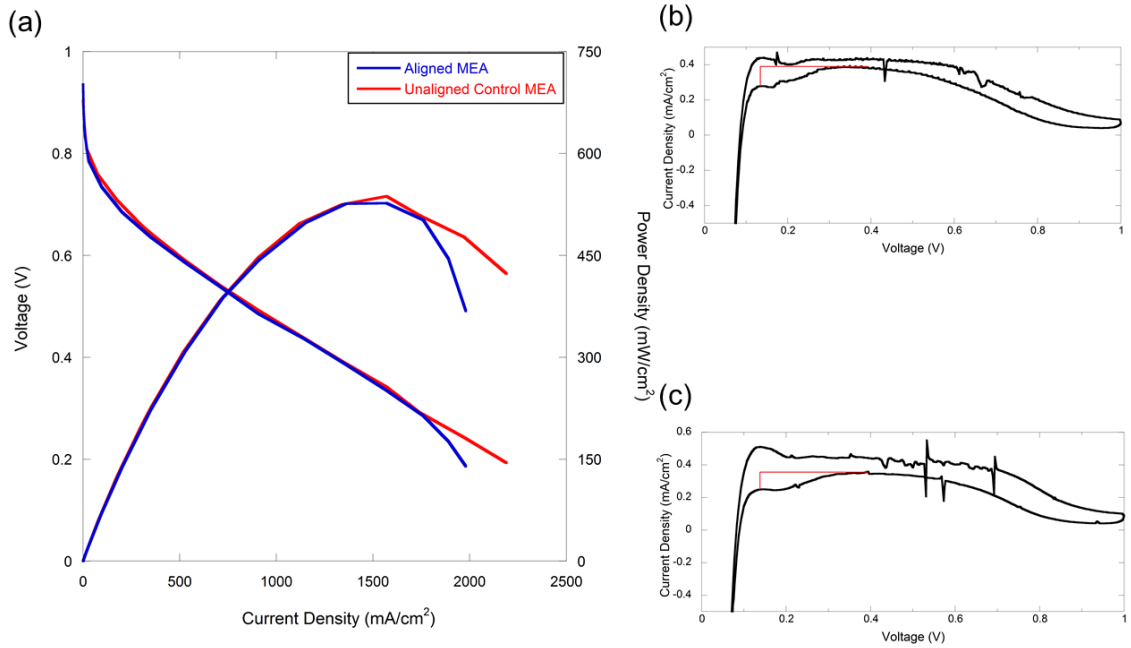


**Figure 4.4** (a) Performance comparison of the aligned MEA and control MEA. CV of the (b) aligned MEA and (c) control MEA.

It is apparent that in this case the fiber alignment in the catalyst layer had no effect on the performance of the MEA. The performance of the MEA is largely dependent on the number of TPBs and the resistance encountered by each species. Based on the ECSA, there was no evidence of increase in the number of TPBs. This is consistent with the SEM images, which showed no significant differences in fiber morphology. Additionally, the alignment did not contribute measurably to species transport resistance as the increase in mass transport resistance is more readily explained by the larger electrospraying agglomerates.

## 4.4. Conclusions

This study showed that MEAs with catalyst layers fabricated *via* simultaneous electrospinning and electospraying with aligned fibers does not affect the fuel cell performance compared to catalyst layers made with random fibers fabricated *via* simultaneous electrospinning and electospraying. The aligned catalyst layer showed identical peak power density and ECSA. The primary reason for this is that no significant change in the fiber morphology occurs. Specifically, the fiber orientation alone does not change the overall porosity of the cell or the number of TPBs.

# 5. SUMMARY AND FUTURE OUTLOOK

## 5.1. Summary

This work demonstrates the fabrication and characterization of aligned fiber proton exchange membrane fuel cell (PEMFC) catalyst layers using simultaneous electrospinning and electrospraying (E/E). Several apparatuses were investigated for their viability in fabricating the catalyst layers. The chosen apparatus was then used to explore the effects of process parameters on the alignment of Nafion nanofibers. Finally, the fuel cell performance of the aligned catalyst layer was investigated.

The accelerated drum apparatus was shown to be the most reliable method to produce the aligned Nafion nanofibers in the catalyst layer of sufficient area for use in the fuel cell. In another study, the dependence of the alignment on the drum speed and solution flow rate was shown. The accelerated drum was found to produce highly aligned fiber mats under a wide range of drum speeds and solution flow rates. In the last study, the fuel cell performance of the aligned catalyst layer was compared to a randomly oriented control. The aligned catalyst layer was shown to have comparable performance to the randomly aligned control. The results of this thesis show that it is possible to fabricate a PEMFC catalyst layer using an accelerated drum; however, the alignment does not significantly alter the fuel cell performance of the catalyst layer.

## 5.2. Future Outlook

Many possibilities exist for expansion on this work. In this study, focus was placed on the fabrication of an aligned catalyst layer and the resulting fuel cell performance. Many questions regarding the morphology of the aligned layer remain unanswered. There are also several opportunities for the optimization of the morphology of the catalyst layer.

The porous space of the catalyst layer was not sufficiently explored in this study. A technique such as nitrogen adsorption could be utilized to explore the changes in the porous space between a randomly aligned catalyst layer and the aligned layer. This is important to the overall performance of the catalyst layer since pore space provides minimal resistance to gas transport in the catalyst layer, but can also increase electrical and ion resistance.

The Nafion content of a catalyst layer is very important to the fuel cell performance. Optimal Nafion content in traditional cast catalyst layers has been explored.[32] The E/E process introduces an additional complexity as both the Nafion content in fiber form and in the electrospray solution can be explored. It is likely that changing the morphology of the fibers will change the optimum Nafion content.

The ability to control fiber deposition beyond an aligned morphology has been explored.[26, 29] This represents an opportunity to further tailor catalyst layers into morphologies which minimize transport resistances while maximizing the triple phase boundaries.

## REFERENCES


1. Grove, W. R., Voltaic Series and the Combination of Gases by Platinum. *London Edinburgh Philosophical Magazine and Journal of Science* **1839,** *14* (86), 127-30.

2. Cohn, E. M., Nasa's Fuel Cell Program. In *Fuel Cell Systems*, American Chemical Society: Washington D.C., **1969**; Vol. 47, pp 1-8.

3. Srinivasan, S. M., Renaut; Stevens, Philippe; Yang, Christopher, Fuel Cells: Reaching the Era of Clean and Efficient Power Generation in the Twenty-First Century. *Annual Review of Energy and the Environment* **1999,** *24* (1), 281-328.

4. Gasteiger, H. A.; Kocha, S. S.; Sompalli, B.; Wagner, F. T., Activity Benchmarks and Requirements for Pt, Pt-Alloy, and Non-Pt Oxygen Reduction Catalysts for Pemfcs. *Applied Catalysis B: Environmental* **2005,** *56* (1–2), 9-35.

5. Middelman, E., Improved Pem Fuel Cell Electrodes by Controlled Self-Assembly. *Fuel Cells Bulletin* **2002,** *2002* (11), 9-12.

6. Snyder, J. D.; Elabd, Y. A., Nafion® Nanofibers and Their Effect on Polymer Electrolyte Membrane Fuel Cell Performance. *Journal of Power Sources* **2009,** *186* (2), 385-392.

7. Baturina, O. A.; Wnek, G. E., Characterization of Proton Exchange Membrane Fuel Cells with Catalyst Layers Obtained by Electrospraying. *Electrochemical and Solid-State Letters* **2005,** *8* (6), A267-A269.

8. Minoru, U.; Syunsuke, K.; Akifumi, Y.; Isamu, U., Pt/C-Electrocatalyst Painting on Polymer Electrolyte Membrane by Electrostatic Spray Deposition. *Japanese Journal of Applied Physics* **2005,** *44* (2L), L322.

9. Benítez, R.; Soler, J.; Daza, L., Novel Method for Preparation of Pemfc Electrodes by the Electrospray Technique. *Journal of Power Sources* **2005,** *151*, 108-113.

10. Chaparro, A. M.; Gallardo, B.; Folgado, M. A.; Martín, A. J.; Daza, L., Pemfc Electrode Preparation by Electrospray: Optimization of Catalyst Load and Ionomer Content. *Catalysis Today* **2009,** *143* (3–4), 237-241.

11. Martin, S.; Garcia-Ybarra, P. L.; Castillo, J. L., Electrospray Deposition of Catalyst Layers with Ultra-Low Pt Loadings for Pem Fuel Cells Cathodes. *Journal of Power Sources* **2010,** *195* (9), 2443-2449.

12. Chaparro, A. M.; Benítez, R.; Gubler, L.; Scherer, G. G.; Daza, L., Study of Membrane Electrode Assemblies for Pemfc, with Cathodes Prepared by the Electrospray Method. *Journal of Power Sources* **2007,** *169* (1), 77-84.

13. Martin, S.; Martinez-Vazquez, B.; Garcia-Ybarra, P. L.; Castillo, J. L., Peak Utilization of Catalyst with Ultra-Low Pt Loaded Pem Fuel Cell Electrodes Prepared by the Electrospray Method. *Journal of Power Sources* **2013,** *229*, 179-184.

14. Martin, S.; Garcia-Ybarra, P. L.; Castillo, J. L., High Platinum Utilization in Ultra-Low Pt Loaded Pem Fuel Cell Cathodes Prepared by Electrospraying. *International Journal of Hydrogen Energy* **2010,** *35* (19), 10446-10451.

15. Chen, H.; Snyder, J. D.; Elabd, Y. A., Electrospinning and Solution Properties of Nafion and Poly(Acrylic Acid). *Macromolecules* **2008,** *41* (1), 128-135.

16. Brodt, M.; Wycisk, R.; Pintauro, P. N., Nanofiber Electrodes with Low Platinum Loading for High Power Hydrogen/Air Pem Fuel Cells. *Journal of The Electrochemical Society* **2013,** *160* (8), F744-F749.

17. Zhang, W.; Pintauro, P. N., High-Performance Nanofiber Fuel Cell Electrodes. *ChemSusChem* **2011,** *4* (12), 1753-1757.

18. Wang, X.; Richey, F. W.; Wujcik, K. H.; Elabd, Y. A., Ultra-Low Platinum Loadings in Polymer Electrolyte Membrane Fuel Cell Electrodes Fabricated Via Simultaneous Electrospinning/Electrospraying Method. *Journal of Power Sources* **2014,** *264*, 42-48.

19. Wang, X.; Richey, F. W.; Wujcik, K. H.; Ventura, R.; Mattson, K.; Elabd, Y. A., Effect of Polytetrafluoroethylene on Ultra-Low Platinum Loaded

Electrospun/Electrosprayed Electrodes in Proton Exchange Membrane Fuel Cells. *Electrochimica Acta* **2014,** *139*, 217-224.

20. Matthews, J. A.; Wnek, G. E.; Simpson, D. G.; Bowlin, G. L., Electrospinning of Collagen Nanofibers. *Biomacromolecules* **2002,** *3* (2), 232-238.

21. Vaz, C. M.; van Tuijl, S.; Bouten, C. V. C.; Baaijens, F. P. T., Design of Scaffolds for Blood Vessel Tissue Engineering Using a Multi-Layering Electrospinning Technique. *Acta Biomaterialia* **2005,** *1* (5), 575-582.

22. Putti, M.; Simonet, M.; Solberg, R.; Peters, G. W. M., Electrospinning Poly(E-Caprolactone) under Controlled Environmental Conditions: Influence on Fiber Morphology and Orientation. *Polymer* **2015,** *63*, 189-195.

23. Li, D.; Wang, Y.; Xia, Y., Electrospinning Nanofibers as Uniaxially Aligned Arrays and Layer-by-Layer Stacked Films. *Advanced Materials* **2004,** *16* (4), 361-366.

24. Teo, W. E.; Ramakrishna, S., Electrospun Fibre Bundle Made of Aligned Nanofibres over Two Fixed Points. *Nanotechnology* **2005,** *16* (9), 1878.

25. Liu, Y.; Zhang, X.; Xia, Y.; Yang, H., Magnetic-Field-Assisted Electrospinning of Aligned Straight and Wavy Polymeric Nanofibers. *Advanced Materials* **2010,** *22* (22), 2454-2457.

26. Grasl, C.; Arras, M. M. L.; Stoiber, M.; Bergmeister, H.; Schima, H., Electrodynamic Control of the Nanofiber Alignment During Electrospinning. *Applied Physics Letters* **2013,** *102* (5), 053111.

27. Jun, K.; Reid, O.; Yanou, Y.; David, C.; Robert, M.; Geoffrey, W. C.; Craighead, H. G., A Scanning Tip Electrospinning Source for Deposition of Oriented Nanofibres. *Nanotechnology* **2003,** *14* (10), 1124.

28. Sun, D.; Chang, C.; Li, S.; Lin, L., Near-Field Electrospinning. *Nano Letters* **2006,** *6* (4), 839-842.

29. Chieh, C.; Limkrailassiri, K.; Liwei, L., Continuous near-Field Electrospinning for Large Area Deposition of Orderly Nanofiber Patterns. *Applied Physics Letters* **2008,** *93* (12), 123111.

30. Rahmani, S.; Rafizadeh, M.; Afshar Taromi, F., Statistical Analysis of Nanofibers Alignment in Magnetic-Field-Assisted Electrospinning Including an Alignment Percentage Formula. *Journal of Applied Polymer Science* **2014,** *131* (23), n/a-n/a.

31. Dong, B.; Gwee, L.; Salas-de la Cruz, D.; Winey, K. I.; Elabd, Y. A., Super Proton Conductive High-Purity Nafion Nanofibers. *Nano Letters* **2010,** *10* (9), 3785-3790.

32. Sasikumar, G.; Ihm, J. W.; Ryu, H., Optimum Nafion Content in Pem Fuel Cell Electrodes. *Electrochimica Acta* **2004,** *50* (2), 601-605.